Chapter 2

DNA-Encoded Antibody Libraries: A Unified Platform for Multiplexed Cell Sorting and Detection of Genes and Proteins

2.1 Introduction

Global genomic and proteomic analyses of tissues are impacting our molecular-level understanding of many human cancers. Particularly informative are studies that integrate both gene expression and proteomic data. Such multi-parameter data sets are beginning to reveal the perturbed regulatory networks which define the onset and progression of cancers (1–5). This new picture of cancer, and the emergence of promising new cancer drugs (6, 7) are placing new demands on clinical pathology (8). For example, traditional pathology practices (i.e. microscopic analysis of tissues) do not distinguish potential responders from non-responders for the new cancer molecular therapeutics (9). Recent examples exist in which pauciparameter molecular measurements are being employed to identify potential responders to at least two

therapauetics (10–13). However, it is unlikely that single-parameter measurements will be the norm. Instead, the coupling of molecular diagnostics with molecular therapeutics will eventually require measurements of a multi-parameter (e.g. cells, mRNAs and proteins) biomarker panel that can be used to direct patients to appropriate therapies or combination therapies.

Currently, the measurement of a multi-parameter panel of biomarkers from diseased tissues requires combinations of microscopic analysis, microarray data (14), immunohistochemical staining, western blots (8), and other methods. The collected data is integrated together within some model for the disease, such as a cancer pathway model (15), to generate a diagnosis. Currently, performing these various measurements requires a surgically resected tissue sample. The heterogeneity of such biopsies can lead to significant sampling errors since various measurements of cells, mRNAs, and proteins are each executed from different regions of the tissue.

In this chapter, the DNA-encoded antibody library, or DEAL, approach (**Figure 2.1**), is described as an important step towards executing a true multi-parameter analysis (cells, mRNAs and proteins) from the same microscopic region of tissue. We report on several key demonstrations for achieving this goal, including the rapid detection of proteins and protein panels over a broad dynamic range and with a detection limit of <10 femtoM; the sorting of immortal and primary lymphocyte populations; the co-detection of cells, cDNAs, and proteins on the same platform, and the integration of our multi-parameter platform with microfluidic techniques.

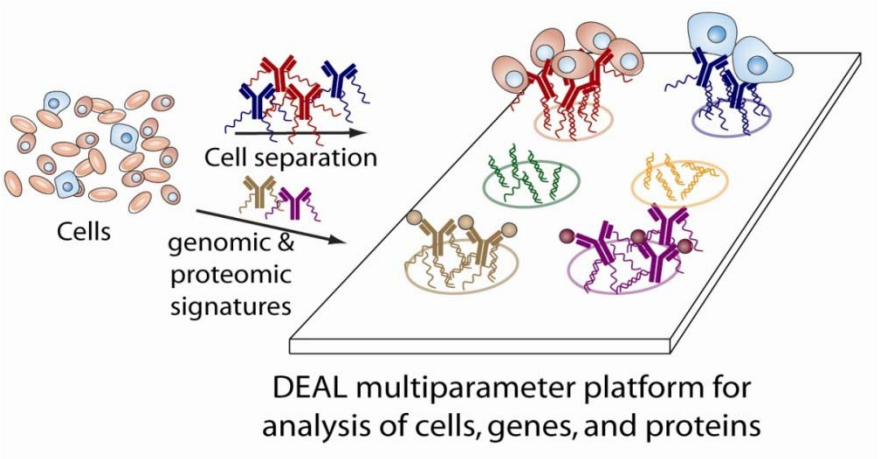

Figure 2.1 Illustration of the DEAL method for cell sorting and co-detection of proteins and cDNAs (mRNAs). Unique DNA-Antibody conjugates are prepared and then combined into a single solution where they recognize cognate antigens, including cell surface markers and proteins of interest. When introduced onto a conventional DNA microarray, parallel self assembly, according to Watson-Crick base pairing, localizes the bound species to a specific spatial location allowing for highly multiplexed multi-parameter analysis.

A key issue involved with a microfluidics-based multi-parameter assay is that the measurement of different classes of biomolecules (or cells) typically requires different surface chemistries, and not all of them are compatible with each other or the fabrication steps associated with building the microfluidics circuitry. Conventional antibody arrays for protein detection or for panning cells (16) require immobilization of the antibody onto aldehyde, epoxy, maleimide, or hydrophobic solid supports (17–20). It is often difficult to preserve folded (active) antibody conformations due to surface induced denaturation which depends on many variables including pH, ionic strength, temperature and concentration (21–23). This has spurred the development of alternative approaches to preserve the native conformation of proteins including 3-dimensional matrixes like hydrogels, and polyacrylamide (24, 25), cutinase-directed antibody immobilization onto SAMs (26), and the coupling of biotinylated antibodies onto streptavidin coated surfaces

(27). In addition, the arrays need to remain hydrated throughout the entire manufacturing process in order to prevent protein denaturation (18). DNA microarrays, on the other hand, are typically electrostatically absorbed (via spotting) unto amine surfaces. One option for detecting both DNA and proteins on the same slide would be to pattern both functional groups used to immobilize DNA and protein onto the same substrate, although this would significantly increase the complexity and engineering of the system. Alternatively, a compatible surface may be an activated ester glass slide to which amine-DNA and proteins can both covalently attach. However, we have found that the loading capacity of these slides for DNA is diminished, resulting in poor signal intensity when compared with DNA printed on conventionally prepared amine slides. In addition, unreacted esters are hydrolyzed back to carboxylic acids, which are negatively charged at normal hybridization buffers (pH 7), electrostatically reducing the DNA interaction. Moreover, to interrogate cells and proteins, the best surface to reduce non specific binding of cells while maintaining full antibody functionality is acrylamide (28, 29), which is incompatible with DNA.

By using DNA as a common assembly strategy for cells, cDNAs, and proteins, we are able to optimize the substrate conditions for high DNA loading onto the spotted substrates, and for complementary DNA loading on the antibodies. This leads to highly sensitive sandwich assays for protein detection, as well as high efficiency cell sorting (compared with traditional panning). We also find that non-selective binding (biofouling) of proteins to DNA-coated surfaces is reduced. Importantly, DNA coated surfaces can be dried out, stored or heated (overnight at 80^{o} C), thus making them compatible with robust microfluidics fabrication.

DNA-labeled antibodies have been previously used to detect proteins (30–32), largely with the pendant oligomers serving as immuno-PCR tags (33, 34). DNA-tags have been used to direct the localization of proteins allowing assays to take advantage of spatial encoding, via several different read-out strategies (35–37). Conventional multi-well ELISA assays are capable of quantitating multiple proteins, but typically require separate sample volumes for each parameter. Optical multiplexing can expand this, but is limited by the number of non-spectrally overlapping chromophores. Spatial multiplexing, such as is used with DEAL, allows for the execution of many measurements on a small sample, since the number of different measurements is limited only by the patterning method utilized to prepare the cDNA array. Spotted antibody arrays (18), while potentially useful for protein detection and/or cell sorting, are not easily adaptable towards microfluidics-based assays, since the microfabrication process for preparing robust microfluidics devices often involves physical conditions that will damage the antibodies. Complementary DNA arrays are robust to such fabrication conditions.

2.2 Experimental Methods

2.2.1 DNA sequences for spatial encoding

All DNA strands were purchased with a 5’-amino modification from the Midland Certified Reagent company. Sequences for sequences A1, B1, C1 and their respective complements A1’, B1’ and C1’ are given in Table 2.1. Computationally derived sequences, designated as A3, B3, C3 and their respective complements A3’, B3’ and C3’ were designed following the paradigm outlined by Dirks et al. (38). Example input files

and output sequences can be found in the Appendix A. The sequences are reported in Table 2.1.

Table 2.1 DNA sequences for spatial encoding

Name	Sequence
A1	5'-NH2-AAAAAAAAAACGTGACATCATGCATG-3'
A1'	3'-GCACTGTAGTACGTACAAAAAAAAAA-NH2-5'
B1	5'-NH2-AAAAAAAAAAGGATTCGCATACCAGT-3'
B1'	3'-CCTAAGCGTATGGTCAAAAAAAAAAA-NH_2-5'
C1	5'-NH_2-AAAAAAAAAATGGACGCATTGCACAT-3'
C1'	3'-ACCTGCGTAACGTGTAAAAAAAAAAA-NH_2-5'
A3	5'-NH_2-AAA AAA AAA A AT CCT GGA GCT AAG TCC GTA
A3'	5'-NH_2- AAA AAA AAA ATA CGG ACT TAG CTC CAG GAT
B3	5'-NH_2-AAA AAA AAA AGC CTC ATT GAA TCA TGC CTA
B3'	5'-NH_2-AAA AAA AAA AGC ACT CGT CTA CTA TCG CTA
C3	5'-NH_2-AAA AAA AAA AGC ACT CGT CTA CTA TCG CTA
C3'	5'-NH_2-AAA AAA AAA ATA GCG ATA GTA GAC GAG TGC

2.2.2 DNA antibody conjugation

AlexaFluor 488, 594, and 647-labeled polyclonal Goat anti-Human IgGs were purchased from Invitrogen. Monoclonal Rabbit anti-Human Interleukin-4 (clone: 8D4-8), non-fluorescent and APC-labeled Rabbit anti-Human Tumor Necrosis Factor-α (clones: MAb1 and MAb11, respectively), and non-fluorescent and PE-labeled Rabbit anti-Human Interferon-γ (clones: NIB42 and 4S.B3, respectively) were all purchased from eBioscience. Non-fluorescent and biotin-labeled mouse anti-Human Interleukin-2

(clones: 5344.111 and B33-2, respectively) were purchased from BD Biosciences. Prior to use, all antibodies were desalted, buffer exchanged to pH 7.4 PBS and concentrated to ~ 1mg/ml using 3000 MWCO spin filters (Millipore). Succinimidyl 4-hydrazinonicotinate acetone hydrazone in DMF (SANH, Solulink) was added to the antibodies at variable molar excess of (1000:1 to 5:1) of SANH to antibody. In this way the number of hydrazide groups introduced to the antibodies was varied. Separately, succinimidyl 4-formylbenzoate in DMF (SFB, Solulink) was added at a 20-fold molar excess to 5'aminated 26mer oligomers in PBS. This ratio of SFB to DNA ensured complete reaction of the 5' amine groups to yield 5' aldehydes. No further improvement in yield was observed for either the antibody and oligonucleotide coupling reactions after 4 hours at room temperature. Excess SANH and SFB were removed and samples buffered exchanged to pH 6.0 citrate buffer using protein desalting spin columns (Pierce). A 20-fold excess of derivatized DNA was then combined with the antibody and allowed to react overnight at room temperature. Non-coupled DNA was removed with size exclusion spin columns (Bio-Gel P-30, Bio-Rad) or purified using a Pharmacia Superdex 200 gel filtration column at 0.5 ml/min isocratic flow of PBS. The synthesis of DNA-antibody conjugates was verified by non-reducing 7.5% Tris-HCl SDS-PAGE at relaxed denaturing conditions of 60^{o}C for 5 minutes, and visualized with a Molecular Imager FX gel scanner (Bio-Rad). Conjugation reactions involving fluorescent antibodies or fluorescentl oligonucleotides were imaged similarly using appropriate excitation and emission filters.

2.2.3 Microarray Fabrication

DNA microarrays were printed via standard methods by the microarray facility at the Institute for Systems Biology (ISB—Seattle, WA) onto amine-coated glass slides. Typical spot size and spacing were 150 and 500 μm, respectively. Poly-lysine slides were made in house. Blank glass slides were cleaned with IPA and water in a sonication bath for 10 minutes each. They were then treated with oxygen plasma at 150 W for 60 sec., and then quickly dipped into DI water to produce a silanol terminated, highly hydrophilic surface. After drying them with a nitrogen gun, poly-L-lysine solution (Sigma P8920, 0.1% w/v, without dilution) was applied to the plasma treated surfaces for 15 minutes, and then rinsed off with DI water for several seconds. Finally, these treated slides were baked at 60^{o}C for 1hr. These slides were then sent to ISB and printed as described above.

2.2.4 Fabrication of Microfluidic Devices

Microfluidic channels were fabricated from polydimethylsiloxane (PDMS) using conventional soft lithographic techniques. The goal was to fabricate robust microfluidics channels that could be disassembled after the surface assays were complete for optical analysis. Master molds were made photolithographically from a high resolution transparency mask (CadArt) so that the resulting fluidic network consisted of 20 parallel channels each having a cross-sectional profile of 10 x 600 μm and were 2 cm long. This corresponds to channel volumes of 120 nl. A silicone elastomer (Dow Corning Sylgard 184) was mixed and poured on top of the mold. After curing, the PDMS was removed from the mold and sample inlet and outlet ports punched with a 20 gauge steel pin

(Technical Innovations). The microfluidic channels were then aligned on top of the microarray and bonded to the substrate in an 80^{o}C oven overnight.

2.2.5 1^{o} Antibody Microarray Generation and DEAL-Based Immunoassays

Antibody microarrays were generated by first blocking the DNA slide with 0.1% BSA in 3x SSC for 30 minutes at 37^{o}C. The slides were washed with dH_2O and blown dry. A 30 μl solution containing DNA-antibody conjugates (3x SSC, 0.1% SDS, 0.1% BSA, 15 ng/μl of each conjugate) was sandwiched to the array with a microscope slide, and incubated at 37^{o}C for 4 hours. Arrays were then washed first in 1x SSC, 0.05% SDS at 37^{o}C with gentle agitation, then at 0.2x SSC, then finally at 0.05x SSC. The slides were blown dry and scanned with a Gene Pix 4200 A two-color array scanner (Axon Instruments). For immunoassays, the DNA-encoded 1^{o} antibody (15 ng/μl), antigen (3 ng/μl) and fluorescent 2^{o} antibody (0.5 ng/μl) were combined in a single tube. After 2 hour incubation at 37^{o}C, the formed antibody-antigen-antibody complexes were introduced to the microarrays as described above. Subsequent wash steps and visualization were identical.

2.2.6 Microfluidic-based assay procedures

Microfluidic devices were interfaced with 23 gauge steel pins and Tygon tubing to allow pneumatically controlled flow rates of ~0.5 μl/min. The assays were performed in Tris Buffered Saline (TBS), which was found to be better than 1x SSC and PBS. Each channel was blocked with 1.0% BSA in TBS prior to exposure to DNA-antibody conjugates or immunoassay pairs for 10 minutes under flowing conditions. After a 10 minute exposure to conjugates or antigens under flowing conditions, channels were

washed with buffer for 2 minutes and the microfluidics disassembled from the glass slide in order to be scanned. Immediately prior to imaging, the entire slide was briefly rinsed in TBS, blown dry and imaged on an array scanner as described above. For the human IL-2 concentration series, primary DNA-antibody conjugates were laid down first on the surface, before exposure to antigen and secondary antibody. This was necessary because at lower concentrations of antigen, the signals decrease, due to the high ratio of antigen-unbound primary antibody competing with antigen-bound primary for hybridization to the DNA array. By first exposing the array to the primary DNA-antibody conjugate, excesses were washed away before subsequent exposure to antigen and secondary antibody, increasing signal.

2.2.7 Microfluidic Au amplification methods

Microfluidics-based Au amplification experiments were performed in a similar manner, with the notable exception that a biotin-secondary antibody was used instead of a fluorescently labeled antibody. Subsequently, Au-streptavidin (Nanoprobes) was introduced into each channel (3ng/μl) for 10 minutes, after which the channels were thoroughly rinsed with buffer. After removal of the PDMS, the entire slide was then amplified with gold enhancer kit (Nanoprobes) according to manufacturer's protocol.

2.2.8 Analysis of DNA-encoded antibodies by flow cytometry

VL3 and A-20 cells were incubated for 20 min. on ice with 0.5 μg of FITC-conjugated Rat Anti-Mouse CD90.2 (Thy1.2, BD Pharmingen, clone 30-H12, catalog # 553012) in 100 μL PBS-3% FCS. Cells were also incubated with equimolar amounts of α-CD90.2/FITC-DNA conjugates characterized by various FITC-DNA loadings. Cells

were washed once with PBS-3% FCS and then were analyzed by flow cytometry on a BD FACSCanto^{TM} instrument running the BD FACSDiva^{TM} software.

2.2.9 Cell capture, separation, and sorting methods

Two murine cell lines, VL-3 T cells (thymic lymphoma line (39)) and A20 B cells (mouse B cell lymphoma (40), purchased from ATCC) were engineered to express mRFP and EGFP, respectively, using standard retroviral transduction protocols. Antibodies against surface markers for each of these cell lines, α-CD90.2 for VL-3 and α-B220 for A20 (eBioscience), were encoded as described above with DNA strands A1' and B1', respectively.

For sorting experiments, cells were passaged to fresh culture media [RPMI 1640 (ATCC) supplemented with 10 % fetal bovine serum, 0.1 mM non-essential amino acids and 0.05 mM β-mercaptoethanol at a concentration of 10^6 cells/100 μl media and incubated with DNA-antibody conjugate (0.5 μg/100 μl) for 30 minutes on ice. Excess conjugate was removed from the supernatant after centrifugation, after which cells were resuspended in fresh media. Prior to cell incubation the microarray slide was passivated, to reduce non-specific cell adhesion, by reaction of the residual amine groups with methyl-PEO_{12}-NHS ester (Pierce) 10 mM in pH = 7.4 PBS for 4 hours at room temperature. Cells were spread evenly across the microarray surface and allowed to localize for one hour on ice. After this period, non-adherent cells were removed with gentle washing with room temperature Tris-buffered saline solution including 1 mM $MgCl_2$. Cell enrichment experiments were performed identically except that all incubation steps were performed in the presence of a 1:1 mixture of both T- and B-cells (each at 10^6/100 μl).

Primary CD4+ and CD8+ T cells were purified from EGFP and dsRed transgenic mice (obtained from Jackson Laboratories), respectively, using standard magnetic bead negative selection protocols and the BD IMagTM cell separation system. Prior to DEAL-based fractionation, the purity of these populations was analyzed by FACS and found to be greater than 80%.

Simultaneous cell, gene and protein experiments were performed similarly to those as previously described on a PEGylated microarray substrate. Briefly, GFP-expressing B cells (10^6/100 μl) were located on B1 spots after labeling with α-B220-B1' (0.5 μg/100μl). Following removal of non-adherent cells, a TNF-α ELISA pair with C1'-encoded 1^o and APC-labeled 2^o antibodies were introduced along with 0.5 ng/μl FITC-labeled A1' and allowed to hybridize for a period of 30 minutes at room temperature. The slide was then rinsed with TBS+$MgCl_2$ and visualized via brightfield and fluorescence microscopy.

Homogeneous and panning cell experiments were performed in parallel. For the homogenous cell capture process, $5x10^6$ Jurkats (ATCC) suspended in 1 ml of RPMI media along with 5 μg of α-CD3/C3' conjugates and incubated on ice for 1 hour. Excess conjugates were removed by centrifugation and the Jurkats were resuspended into 200 μl of fresh media before exposure to the DNA microarray. After 1 hour incubation on ice, the slides were rinsed gently with TBS. The cell panning experiments were performed in parallel; 5 ug of α-CD3/C3' conjugate in 1 ml RPMI media was incubated on a microarray for 1 hour on ice before rinsing in 0.5x PBS, then deionized water. The slide was not blown dry, but gently tapped on the side to remove the majority of the excess

solution, keeping the array hydrated. Jurkats ($5x10^6$/200 μL) were immediately placed on the array for one hour on ice. Subsequent wash and visualization steps are identical.

2.3 Results and Discussion

2.3.1 *In silico* design of orthogonal DNA oligonucleotides

The pendant DNA oligonucleotides were designed *de novo* in order to minimize inter- and intra-strand cross hybridization. We followed the paradigm outlined by Dirks et al. (38) to computationally derive a set of orthogonal 30mers. These sequences were designed with a polyA_{10} sequence followed by a variable 20mer encoding region. The polyA_{10} stretch was incorporated to provide molecular flexibility and to prevent steric hindrance between the 20mer encoding region and the antigen binding domains of the antibody after conjugation. Three sequences, designated A3–C3 were generated using this approach and were tested empirically. Identical cDNA arrays printed with A3, B3, and C3 were probed with fluorescent complements A3' (green), A3'+B3' (red), and A3'+C3' (red). Minimal noise was observed between the probe sequences and noncomplementary spots (**Figure 2.2)**. We performed initial DEAL experiments with sequences A1–C1 before determining that a rational design of the sequences was necessary to minimize noise. Therefore the majority of the experiments outlined in this chapter are presented using sequences A1–C1.

One advantage of using DNA oligonucleotides as molecular addresses is modularity. One working orthogonal set of sequences that has been experimentally validated can be used interchangeably with distinct sets of antibody libraries without modification of the underlying cDNA microarray. This feature allows

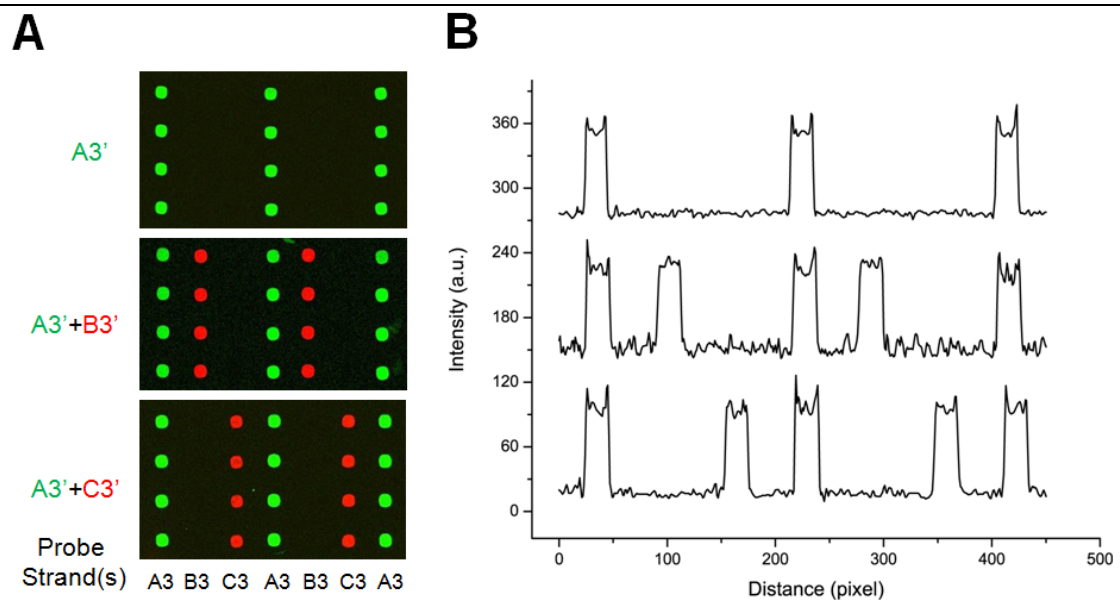

Figure 2.2 DNA sequences derived from computation minimize cross hybridization. (A) Fluorescent scans of three identical cDNA arrays probed with different combinations of fluorescent complementary strands. (B) Intensity profiles of the arrays

2.3.2 Generation of DNA-Antibody conjugates

Chemically modified antibodies to aid in protein immobilization and/or detection are nearly universal for use in immunoassays. Such labeling introduces the risk of detrimentally affecting antibody function; however, that risk can be reduced by minimizing the size, and thus the steric hindrance, of the pendant moieties. With this in mind, we employed a covalent conjugation strategy in which 5'-aminated single-stranded oligonucleotides were coupled to antibodies via a hydrazone linkage (31), as shown in Scheme 2. Using commercially available reagents, an aldehyde functionality was introduced to the 5'-aminated oligonucleotide via succinimide chemistry. Similarly, a hydrazide moiety was introduced via reaction with the lysine side chains of the respective antibody. DNA-antibody conjugate formation was then facilitated via stoichiometric

hydrazone bond formation between the aldehyde and hydrazide functionalities. Conjugate formation and control over DNA-loading (41) was verified by PAGE electrophoresis, as shown in **Figure 2.3.**

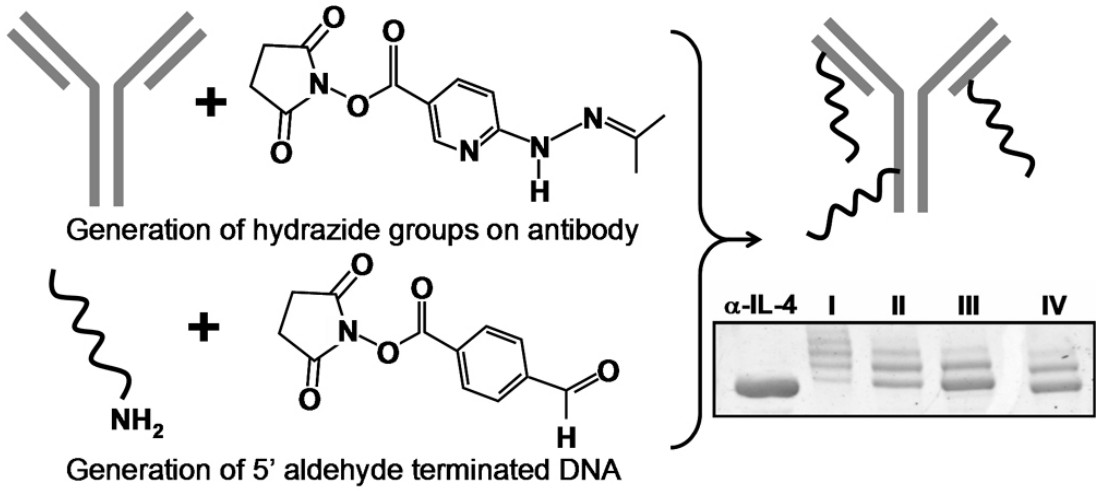

Figure 2.3 Illustration of the two step coupling strategy utilized to prepare DEAL antibodies. In parallel, hydrazide groups are introduced onto a monoclonal antibody and 5' aldehyde modified single-stranded DNA is prepared from 5' aminated oligomers. When combined, hydrazone bonds are formed, linking the ssDNA to the antibody. At bottom right is a gel mobility shift assay showing varied oligomer (strand A1') loading unto α-human IL-4. By varying the stoichiometric ratios of SANH to antibody (lanes **I-IV** corresponds to 300:1, 100:1, 50:1, 25:1 respectively), the average number of attached oligonucleotides can be controlled.

Clearly the adverse steric effects of tagging antibodies with oligonucleotides are of concern when performing various assays, such as the immunoassays and cell sorting/capture experiments described herein. For this reason, we investigated the ability of DNA-encoded antibodies to retain recognition of cell surface markers, as visualized by fluorescence activated cell sorting (FACS). By using a fluorophore covalently tagged to the DNA, but *not* the antibody, FACS was used to optimize DNA-loading for the DEAL conjugates. For the analysis, 5' aminated, 3' FITC-labeled DNA as tagged unto α-CD90.2 antibodies at various stoichiometric ratios of SANH to antibody (5:1, 25:1, 50:1, 100:1, 300:1). This produced, on average, conjugates with 1, 2, 3, 4–5 and 6–7 strands of

FITC-DNA respectively, as measured by gel mobility shift assays (**Figure 2.3**). These conjugates were tested for their ability to bind to the T cell line VL3 (CD90.2 expressing), by monitoring the FITC fluorescence with the flow cytometer. The B cell line A20 (CD90.2 negative) was used as a negative control. The performance of the conjugates was also compared with commercially available FITC α-CD90.2. The results are shown in **Figure 2.4**. The histogram of the mean fluorescent intensities for various FITC-DNA loadings shows that fluorescence increases are roughly linear when the number of DNA strands is increased from 1 to 2 to 3, corresponding to 1, 2 and 3 chromophores (1 per strand). At higher loadings, the increase in fluorescence first plateaus (4–5 oligomers) and then decreases up to the highest loading (6–7 oligomers). Thus, excess DNA labels (4–7 oligomers) did sterically reduce the ability of antibodies to recognize cell surface markers. Optimal loading for cell surface marker recognition was achieved with antibodies synthesized with the 50:1 SANH:antibody ratio, corresponding to approximately three DNA strands per antibody. Subsequent cell sorting experiments were performed in consideration of this observation. When compared with the FITC α-CD90.2 control, the DNA antibody conjugates had reduced fluorescence by a factor of 10 and slightly higher nonspecific binding to A20 cells.

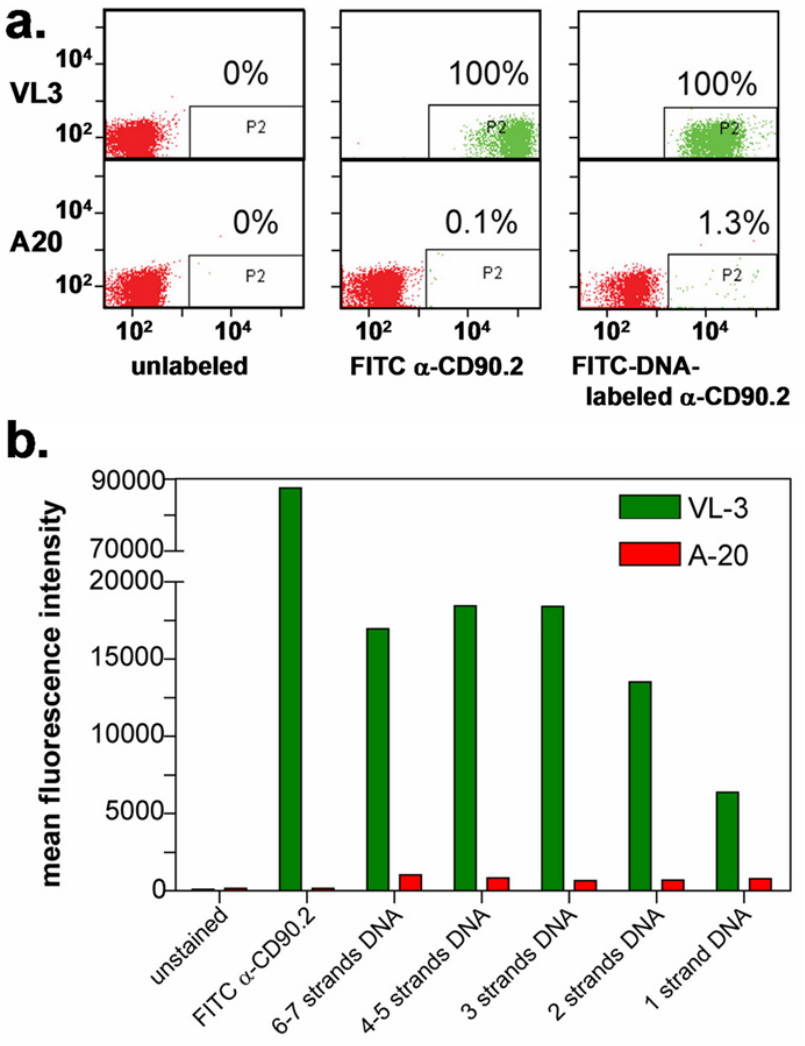

Figure 2.4 Optimization of DNA loading of DEAL antibodies for cell surface marker recognition. (a) FACS plot comparing α-CD90.2/FITC-DNA conjugates with the commercially available FITC α-CD90.2 antibody (no DNA). The conjugates bind to VL3 cells (100%) with minimal non-specific interactions with A20 (1.3%). When compared with FITC α-CD90.2, the overall fluorescent intensities are lower by a factor of 10, with slightly higher non-specific binding to A20. (b) Histogram of the mean fluorescent intensities for various FITC-DNA loadings. Fluorescence increases are roughly linear when the number of DNA strands is increased from 1 to 2 to 3, corresponding to the 1, 2 and 3 chromophores (1 per strand). For higher loadings, the fluorescence plateaus and then decreases.

This could be due to a couple of reasons. A likely factor is that the stoichiometric ratio of fluorophore to antibody for the DEAL conjugates versus the commercial antibody is different. For the DEAL conjugates, each strand of DNA is attached to one fluorophore only (i.e. conjugates with one DNA strand has a fluorophore to antibody ratio of 1:1) whereas the commercial antibodies generally have more than one fluorophore per antibody (i.e. fluorescent antibodies have a fluorophore to antibody ratio >1). Thus the factor of 10 less fluorescence should not be strictly interpreted as a 10x reduction in the binding affinity of the DEAL conjugates, although it is possible that the oligomer steric effects discussed earlier do account for some reduction in relative fluorescence intensity. Direct measurement of the affinity of the DEAL conjugate compared with the corresponding unmodified antibody using methods like Surface Plasmon Resonance (SPR) will be more conclusive.

2.3.3 Multiplexed protein detection by DEAL

We demonstrated the DEAL concept for spatially localizing antibodies using three identical goat anti-human IgGs, each bearing a different molecular fluorophore and each encoded with a unique DNA strand. A solution containing all three antibodies was then introduced onto a microarray spotted with complementary oligonucleotides. After a two hour hybridization period and substrate rinse, the antibodies self-assembled according to Watson-Crick base-pairing, converting the >900 spot complementary DNA chip into a multi-element antibody microarray (**Figure 2.5**). This observation implied that quite large antibody arrays can be assembled in similar fashion.

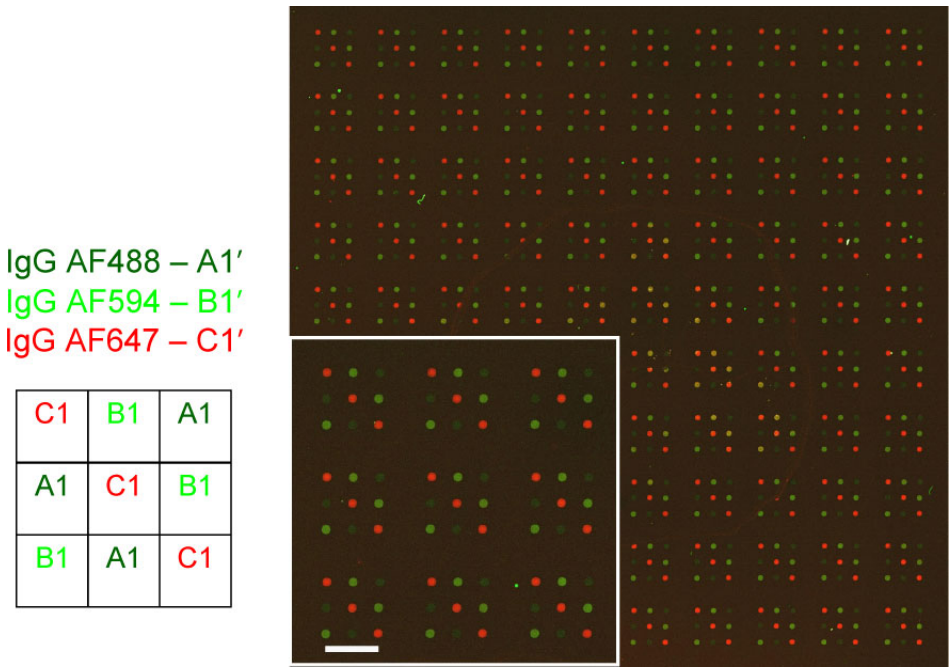

Figure 2.5 Spatially encoded protein array. Three biochemically identical goat α-human IgG (labeled with Alexa488, Alexa594, or Alexa 647 dyes) were tagged with oligos A1', B1' and C1' respectively. After a 2 hour incubation, antibody/DNA conjugates were localized to specific sites dictated by the underlying DNA microarray. Scale bar corresponds to 1 mm.

The ultimate size of any protein array, however, will likely be limited by interference from non-specific binding of proteins. In an effort to visualize the contributions of non-specific binding, three antibodies were similarly introduced onto a microarray: two antibodies having complementary DNA-labeling spotted oligonucleotides and a third unmodified antibody (**Fig. 2.6**). For demonstration purposes, the slide was not thoroughly rinsed following hybridization and accordingly a high background signal due to non-specific adsorption of non-encoded fluorescently-labeled antibody was observed. The spotted nucleotide regions, to which no antibody was chemically encoded, displayed much less non-specifically attached protein, implying that

DNA greatly diminishes active area biofouling. Such retardation of biofouling is reminiscent of substrates that are functionalized with polyethyleneglycol (PEG) (41–43). By analogy with postulated mechanisms associated with PEG (44–46), we hypothesize that the hydrophilic nature of the spotted oligonucleotides minimizes interactions with hydrophobic portions of proteins often exposed during non-specific adsorption. Conjugate hybridization experiments were also carried out within 5 degrees of the calculated duplex melting temperatures, taking advantage of Watson-Crick stringencies and thus diminishing non-complementary DNA interactions. In any case, this reduced biofouling means that the DEAL method can likely be harnessed to detect reasonably large panels of proteins within a single environment.

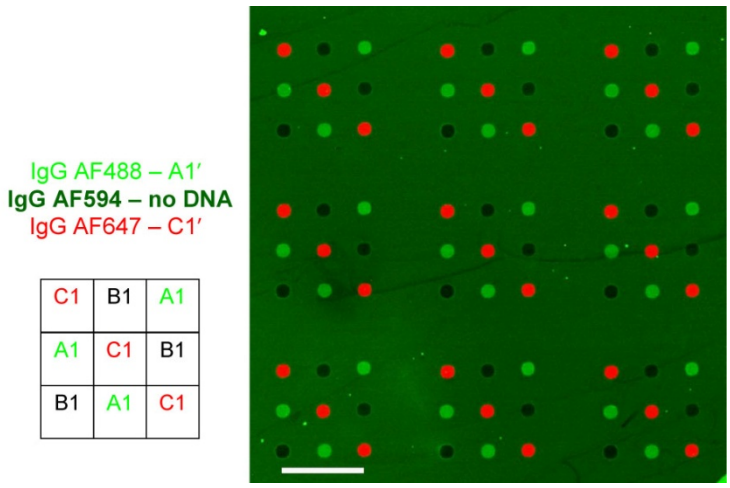

Figure 2.6 Illustration of the resistance of the DEAL approach towards non-specific protein absorption. A microarray was simultaneously exposed to goat α-human IgG-Alexa488/A1', goat α-human IgG-Alexa647/C1' DEAL conjugates and goat α-human IgG-Alexa594 with *no* pendant DNA. When the arrays were not fully blocked and/or rinsed, non-specific binding was observed on the surface of the glass slide, but not on the non-complementary spots of printed DNA, i.e., spot B1 did not have fluorescence from non-complementary IgG conjugates nor did it exhibit fluorescence from proteins not encoded with DNA (goat α-human IgG-Alexa594). Scale bar corresponds to 1mm.

2.3.4 Detection of multiple proteins within a single microfluidic channel

Microfluidic-based assays offer advantages such as reduced sample and reagent volumes, and shortened assay times (47). For example, under certain operational conditions, the surface binding assay kinetics are primarily determined by the analyte (protein) concentration and the analyte/antigen binding affinity, rather than by diffusion (48). We evaluated a microfluidics-based DEAL approach by bonding a polydimethylsiloxane (PDMS)-based microfluidic channel on top of a DNA microarray (**Figure 2.7A**). We initially performed a multiplexed antibody localization experiment, similar to that described above. The antibody conjugates self-assembled at precise spatial locations encoded by the pendant oligonucleotide in <10 minutes (**Figure 2.7B**), consistent with the time scales reported on DNA hybridization in microfluidics (49–51).

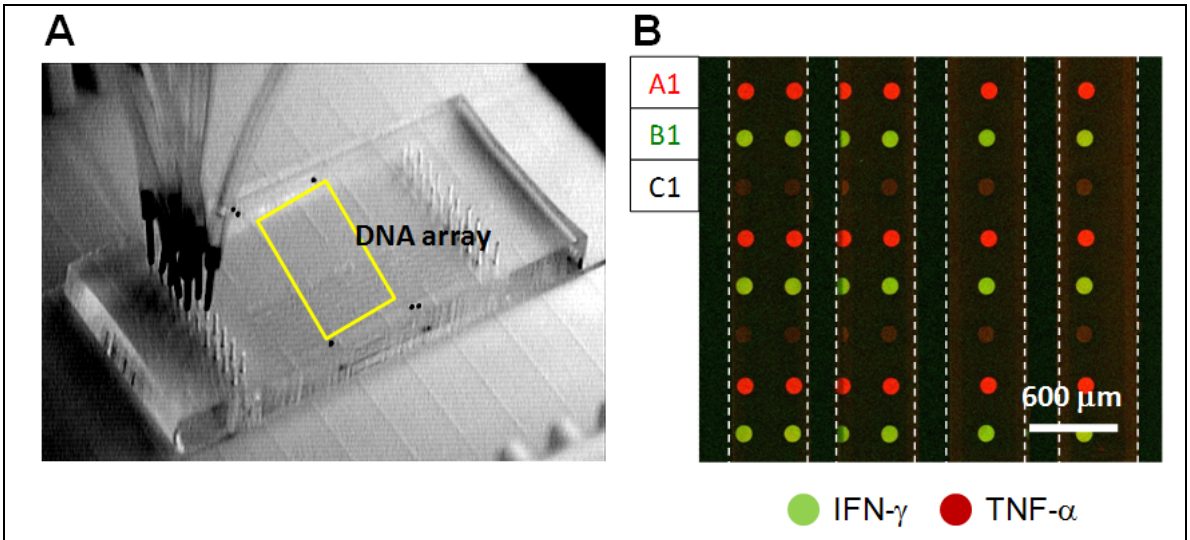

Figure 2.7 Protein array assembled in microfluidics in 10 minutes. (A) Picture of PDMS microfluidic device encapsulated a DNA array (yellow box) (B) Two goat α-human IgG (labeled with Alexa594 or Alexa 647) were tagged with oligos A1' and B1' respectively and introduced into a microfluidic device bonded on top of a DNA microarray with corresponding complementary strands A1 and B1 along with non-complementary strand C1. No DEAL conjugate encoded to spot C1 was added. After flowing at ~0.5 µl/min for 10 minutes, the

microfluidic PDMS slab was removed and the glass slide imaged. The dashed lines delineate separate microfluidic channels of 600 μm width.

To validate the DEAL strategy for protein detection, we utilized encoded antibodies to detect cognate antigens in a variant of standard immunoassays. In a standard immunoassay (52), a primary antibody is adsorbed onto a solid support, followed by the sequential introduction and incubation of the antigen-containing sample and secondary labeled "read-out" antibody, with rinsing steps in between. In order to simplify this conventional five step immunoassay, we reasoned that the encoding power of the DEAL antibodies could serve to position the entire sandwich complex to the appropriate location for multiplexed readout, reducing the assay to a single step. To test this concept, in the same solution, a non-fluorescent, DNA-encoded 1^{o} antibody was combined with antigen and a fluorescently-labeled (no DNA) 2^{o} antibody. Under these conditions, a fluorescent signal will be spatially encoded only if an antibody-antigen-antibody sandwich is successfully formed in homogeneous solution and localized onto the microarray. Upon introduction of DNA-encoded antibodies against two cytokines, human IFN-γ and TNF-α, cognate antigens and fluorescently-labeled 2^{0} antibodies, the DEAL sandwich assays self-assembled to their specific spatial locations where they were detected, as shown in **Figure 2.8**. This multi-protein immunoassay also took 10 minutes to complete.

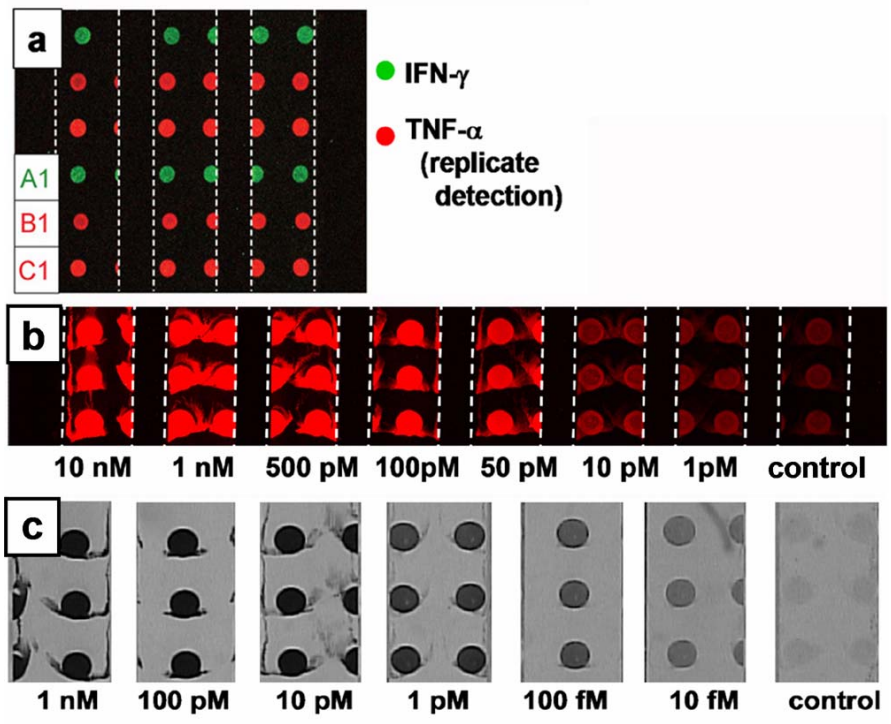

Figure 2.8 DNA-templated protein immunoassays executed within microfluidic channels. The 600 μm micrometer wide channels are delineated with white dashed lines. (a). Two parameter DEAL immunoassay showing the detection of IFN-γ at spot A1 with a PE labeled 2^o antibody (green channel) and replicate detection of TNF-α at spots B1 and C1 with an APC labeled 2^o antibody (red channel). (b) Human IL-2 concentration series visualized using a fluorescent 2^o antibody for detection. (c) Human IL-2 concentration series developed using Au electroless deposition as a visualization and amplification strategy.

We explored the sensitivity limits of a microfluidics, DEAL-based sandwich immunoassay, using a third interleukin, IL-2. Using a fluorescent readout strategy, the assay peaked with a sensitivity limit of around 1 nM on slides printed at saturating concentrations of 5 μM of complementary DNA. Several strategies were employed to increase the sensitivity. First, we reasoned that increasing the loading capacity of the glass slide for DNA will increase the density of DEAL conjugates localized and therefore, increase the number of capture events possible. Conventional DNA microarrays are printed on primary amine surfaces generated by reacting amine-silane

with glass (53). DNA strands are immobilized through electrostatic interactions between the negative charges on the phosphate backbone of DNA and the positive charges from the protonated amines at neutral pH conditions. To increase the loading capacity of the slide, we generated poly-lysine surfaces, increasing both the charge density as well as the surface area of interaction with DNA. By adopting these changes, it became possible to print complementary DNA at saturating concentrations of 100 μM on the glass slides. Correspondingly, the sensitivity of the fluorescent based assays increased to 10 pM (**Figure 2.8b**). In addition, we chose to employ Au nanoparticle-labeled 2^{o} antibodies, followed by electroless metal deposition (54), to further amplify the signal and transform a florescence based read out to an optical one. This is possible since spatial, rather than colorimetric multiplexing, is utilized. Adopting these improvements, the presence of IL-2 interleukin can be readily detected at a concentration limit less than 10 fM (**Figure 2.8c**), representing at least a 1000-fold sensitivity increase over the fluorescence based microfluidics immunoassay. In comparison, this method is 100–1000-fold more sensitive than conventional ELISA (55), and 150 times more sensitive than the corresponding human IL-2 ELISA data from the manufacturer (56).

In performing these experiments, the idea of a 1 step immunoassay was revised. The sensitivity of the assays was reduced when performing a 1 step immunoassay, especially at lower concentrations of antigen. This is most likely due to competitive binding between DEAL conjugates with and without cargo for hybridization unto the underlying DNA microarray. By sequentially exposing the array to DEAL conjugate, antigen, and then secondary antibody, the sensitivities were increased. This is a clear trade off between convenience and sensitivity. It should still be stressed however, that

maximum signal is still reached under microfluidic flowing conditions within 10 minutes for each step. Thus in a fully automated device, a complete microfluidic immunoassay with sensitivities down to 10 fM can be obtained in 1 hour (including a 30 minute step for Au amplification).

In addition to the sample size and time-scale benefits that accompany this type of microfluidics immunoassay, there are other advantages. For example, since the entire assay is performed in solution prior to read-out, protein denaturation (a concern for spotted antibody microarrays) does not reduce binding efficiency. In addition, any assay that involves substrate-supported antibodies, would not have survived microfluidic chip assembly (which involved an extended bake at 80^{o}C). That procedure was designed to yield robust PDMS microfluidics channels that could then be disassembled for the optical readout step. Another benefit of performing solution phase assays is that the orientational freedom enjoyed by both the antigens and antibodies ensures that the solid support will not limit the access of analytes to the binding pocket of the capture agent. We explore this issue in further detail below in the section of cell sorting. Other improvements, such as reducing the DNA spot size (57), and removing spot redundancy are currently being investigated to further lower detection limits.

2.3.5 Multiplexed sorting of immortalized and primary immune cells

We extended the DEAL technique for multiplexed cell sorting. The most common method for cell sorting is FACS, which is well-suited for many applications. Unfortunately, cells separated by conventional FACS are not immediately available for post-sorting analysis of gene and/or protein expression. In addition, FACS is also limited by the number of spectrally distinct fluorophores that can be utilized to label the cell

surface markers used for the sorting. FACS, however, is robust in sorting cells according to multiple cell surface markers. Amongst other alternative cell sorting strategies, the traditional panning method, in which cells interact with surface marker-specific antibodies printed onto an underlying substrate (58), is particularly relevant. Panning is capable of separating multiple cell populations, but has the same limitations as conventional spotted protein microarrays, namely that antibodies are not always oriented appropriately on a surface, and they can also dry out and lose functionality. DEAL overcomes this limitation, by keeping all reagents in solution.

We compared DEAL-based cell sorting with panning by evaluating homogeneous cell capture (solution phase cell capture) and heterogeneous capture of cells (surface confined cell capture). The homogeneous DEAL method exhibited higher cell capture efficiency as shown in **Figure 9a,b**. The increase in capture efficiency can be attributed to several factors. In homogeneous cell capture, the DEAL conjugates are allowed to properly orient and bind to the cell surface markers in solution. Cell capture is not driven by antibody to cell surface marker interactions, but rather by the increased avidity of the multivalent DEAL conjugates for the complementary DNA strands on the microarray through cooperative binding, greatly increasing capture efficiency. Similar trends have been reported for nanoparticle, DNA hybridization schemes (59). With this process, it is typical to see a DNA spot entirely occupied by a confluent layer of cells. With panning methods, which are analogous to our (heterogeneous) DEAL defined arrays, the capture agents are restricted to adopt a random orientation on the surface. The activity of the antibodies is reduced, simply because of improper orientation for interaction with the cell

surface markers, decreasing maximum avidity and cooperation with neighboring antibodies.

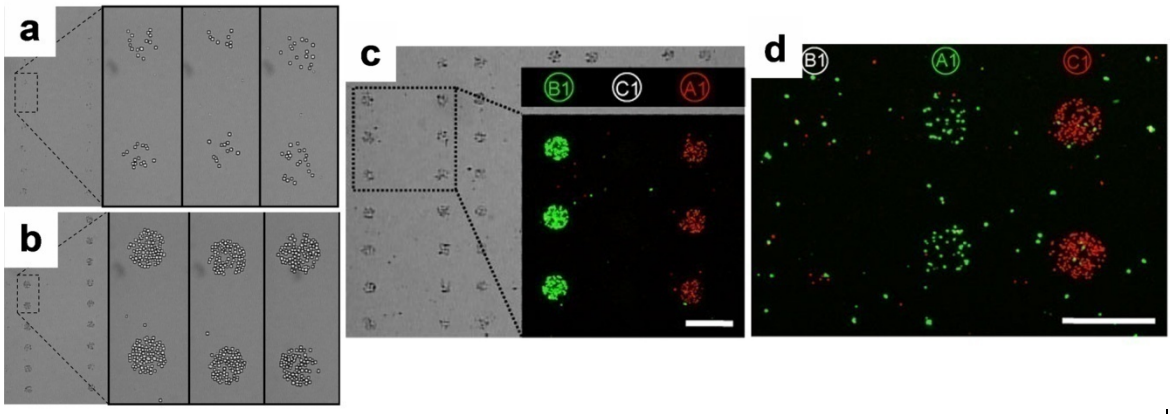

Figure 2.9 Optimization and use of DEAL for multiplexed cell sorting. Panels a and b are brightfield images showing the efficiency of the homogeneous DEAL cell capture process. (a) DEAL labeled antibodies are first assembled onto a spotted DNA array, followed by introduction of the cells. This heterogeneous process is similar to the traditional panning method of using surface bound antibodies to trap specific cells. (b) A homogeneous assay in which DEAL labeled antibodies are combined with the cells, and then the mixture is introduced onto the spotted DNA array microchip. This process is clearly much more efficient. Brightfield and fluorescence microscopy images of multiplexed cell sorting experiments where a 1:1 mixture of mRFP-expressing T cells (red channel) and EGFP-expressing B cells (green channel) is spatially stratified onto spots A1 and B1, corresponding to the encoding of α-CD90.2 and α-B220 antibodies with A1' and B1', respectively. (c) Fluorescence micrograph of multiplexed sorting of primary cells harvested from mice. A 1:1 mixture of CD4+ cells from EGFP transgenic mice and CD8+ cells from dsRed transgenic mice are separated to spots A1 and C1 by utilizing DEAL conjugates α-CD4-A1' and α-CD8-C1', respectively.

We also investigated the use of DEAL for multiplexed cell sorting. Two unique DNA strands were conjugated to antibodies raised against the T cell marker CD90.2 (Thy1.2) and the B cell marker CD45R (B220), respectively. Multiplexed DEAL-based cell sorting was demonstrated by spatially separating a 1:1 mixture of monomeric Red fluorescent protein (60) (mRFP)-expressing T cells (VL-3, murine thymic lymphoma) and EGFP-expressing B cells (mouse B cell lymphoma). This mixture was incubated

with uniquely encoded DNA-antibody conjugates against both T and B cell markers and introduced to an appropriately spotted microarray. **Figure 2.9c** shows both brightfield and false color fluorescence micrographs demonstrating that the mRFP-expressing T cells are enriched at spots A1 and EGFP-expressing B-cells located at B1, consistent with the DNA-encoding of the respective antibodies.

Primary cells are usually more fragile than established cell lines. This is due to the fact that they have to be extracted (usually by enzymatic digestions) from the surrounding tissues, a process that can lead to decreased viability. Moreover, the culture process often selects for clones characterized by greatly increased viability as well as proliferation potential. A generalized cell sorting technology must therefore also work on primary cells with minimal sample manipulation. To demonstrate the utility of DEAL for primary cell sorting, a synthetic mixture of CD4+ and CD8+ T cells was isolated via magnetic negative depletion from EGFP- and dsRED- transgenic mice, respectively. The mixture was stratified using α-CD4 and α-CD8 DNA-antibody conjugates. As shown in **Figure 2.9d**, the two cell types were separated to different spatial locations according to the pendant DNA encoding.

2.3.6 Single environment detection of specific cDNAs, proteins and cells

To highlight the universal diversity of this platform, GFP-expressing B cells were tagged with B1' DNA-encoded antibody conjugates and spatially located onto spots (B1) encoded with the complementary oligonucleotide. Post cell localization, FITC-labeled A1' DNA and a C1'-encoded TNF-α immunosandwich, were combined and introduced to the same microarray platform. The resulting brightfield and fluorescence microscopy

images, shown in **Figure 2.10**, demonstrate the validity of the DEAL platform for simultaneously extending across different levels of biological complexity.

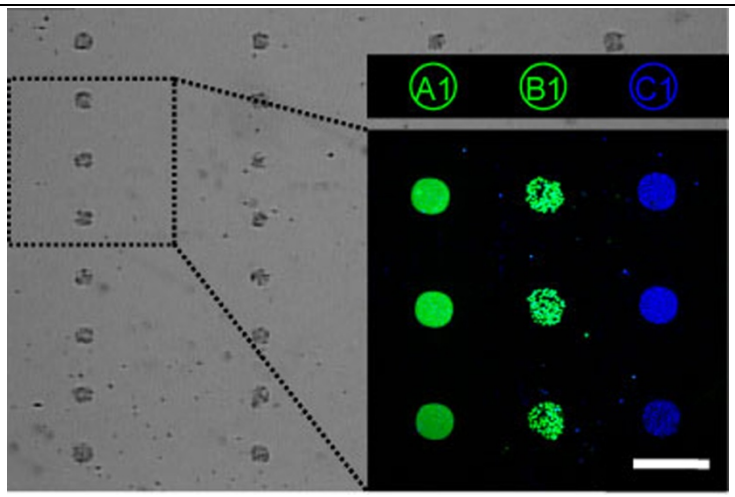

Figure 2.10 Microscopy images demonstrating simultaneous cell capture at spot B1 and multi-parameter detection of genes and proteins, at spots A1 and C1, respectively. The brightfield image shows EGFP-expressing B cells (green channel) located to spots B1, FITC-labeled (green) cDNA at A1, and an APC-labeled TNF-α sandwich immunoassay (blue) encoded to C1. The scale bar corresponds to 300 μm.

2.4 Conclusions

By utilizing DNA as a universal linkage we have demonstrated a platform capable of simultaneous cell sorting, ssDNA and protein detection. DEAL represents a promising approach for the large scale, multi-parameter analysis of biological samples. We are currently applying DEAL towards the separation of highly complex primary cell mixtures such as whole mouse spleen and whole mouse thymus extracts. In addition, microfluidics-based DEAL immunoassays arrays are currently being harnessed for the analysis of protein biomarker panels from mouse whole-blood. We are particularly interested in integrating DEAL with advanced, on chip tissue handling tasks followed by simultaneous quantitation of mRNAs and proteins, because this is where DEAL can

potentially assist in pathological analysis of cancerous tissues. From a more fundamental cancer biology perspective, a near-term targeted application is the capture and functional evaluation of tumor-specific cytotoxic lymphocytes (28, 61). Such an application requires both rare cell capture, cell activation, and the subsequent detection of secreted proteins. For such problems, DEAL has the potential to eliminate any adverse effects of sample dilution and can thus greatly simplify the analysis of the biological system.

2.5 References

1. Lin, B.; White, J. T.; Lu, W.; Xie, T.; Utleg, A. G.; Yan, X.; Yi, E. C.; Shannon, P.; Khretbukova, I.; Lange, P. H.; Goodlett, D. R.; Zhou, D.; Vasicek, T. J.; Hood, L. Evidence for the presence of disease-perturbed networks in prostate cancer cells by genomic and proteomic analyses: a systems approach to disease. *Cancer Res.* **2005**, *65*, 3081–3091.

2. Kwong, K. Y.; Bloom, G. C.; Yang, I.; Boulware, D.; Coppola, D.; Haseman, J.; Chen, E.; McGrath, A.; Makusky, A. J.; Taylor, J.; Steiner, S.; Zhou, J.; Yeatman, T. J.; Quackenbush, J. Synchronous global assessment of gene and protein expression in colorectal cancer progression. *Genomics* **2005**, *86*, 142–158.

3. Huber, M.; Bahr, I.; Kratzchmar, J. R.; Becker, A.; Muller, E.-C.; Donner, P.; Pohlenz, H.-D.; Schneider, M. R.; Sommer, A. Comparison of proteomic and genomic analyses of the human breast cancer cell line T47D and the antiestrogen-resistant derivative T47D-r. *Molec. Cell. Proteomics* **2004**, *3*, 43–55.

4. Tian, Q.; Stepaniants, S. B.; Mao, M.; Weng, L.; Feetham, M. C.; Doyle, M. J.; Yi, E. C.; Dai, H.; Thorsson, V.; Eng, J.; Goodlett, D.; Berger, J. P.; Gunter, B.; Linseley, P. S.; Stoughton, R. B.; Aebersold, R.; Collins, S. J.; Hanlon, W. A.; Hood, L. E. Integrated genomic and proteomic analyses of gene expression in Mammalian cells. *Molec. Cell. Proteomics* **2004**, *3*, 960–969.

5. Chen, G.; Gharib, T. G.; Huang, C.-C.; Taylor, J. M. G.; Misek, D. E.; Kardia, S. L. R.; Giordano, T. J.; Iannettoni, M. D.; Orringer, M. B.; Hanash, S. M.; Beer, D. G. Discordant protein and mRNA expression in lung adenocarcinomas. *Molec. Cell. Proteomics* **2002**, *1*, 304–313.

6. Prados, M.; Chang, S.; Burton, E.; Kapadia, A.; Rabbitt, J.; Page, M.; Federoff, A.; Kelly, S.; Fyfe, G. *Proc. Am. Soc. Clin. Oncology* **2003**, *22*, 99.

7. Rich, J. N.; Reardon, D. A.; Peery, T.; Dowell, J. M.; Quinn, J. A.; Penne, K. L.; Wikstrand, C. J.; van Duyn, L. B.; Dancey, J. E.; McLendon, R. E.; Kao, J. C.; Stenzel, T. T.; Rasheed, B. K. A.; Tourt-Uhlig, S. E.; Herndon, J. E.; Vredenburgh, J. J.; Sampson, J. H.; Friedman, A. H.; Bigner, D. D.; Friedman, H. S. Phase II trial of gefitinib in recurrent glioblastoma. *J. Clin. Oncology* **2004**, *22*, 133–142.

8. Mellinghoff, I. K.; Wang, M. Y.; Vivanco, I.; Haas-Kogan, D. A.; Zhu, S.; Dia, E. Q.; Lu, K. V.; Yoshimoto, K.; Huang, J. H. Y.; Chute, D. J.; Riggs, B. L.; Horvath, S.; Liau., L. M.; Cavenee, W. K.; Rao, P. N.; Beroukhim, R.; Peck, T.

C.; Lee, J. C.; Sellers, W. R.; Stokoe, D.; Prados, M.; Cloughesy, T. F.; Sawyers, C. L.; Mischel, P. S. Molecular Determinants of the Response of Glioblastomas to EGFR Kinase Inhibitors. *N. Engl. J. Med.* **2006**, *353*, 2012–2024.

9. Betensky, R. A.; Louis, D. N.; Cairncross, J. G. Influence of unrecognized molecular heterogeneity on randomized clinical trials. *J. Clin. Oncology* **2002**, 20, 2495–2499.

10. Hughes, T.; Branford, S., 2003. *Semin Hematol.* 2 Suppl 2, 62–68.

11. Lamb, J.; Crawford, E. D.; Peck, D.; Modell, J. W.; Blat, I. C.; Wrobel, M. J.; Lerner, J.; Brunet, J. P.; Subramanian, A.; Ross, K. N.; Reich, M.; Hieronymus, H.; Wei, G.; Armstrong, S. A.; Haggarty, S. J.; Clemons, P. A.; Wei, R.; Carr, S. A.; Lander, E. S.; Golub, T. R. The Connectivity Map: using gene-expression signatures to connect small molecules, genes, and disease. *Science* **2006**, *313 (5795)*, 1929–1935.

12. Martin, M. Molecular biology of breast cancer. *Clin. Transl Oncol. 8 (1)*, 7–14.

13. Radich, J. P.; Dai, H.; Mao, M.; Oehler, V.; Schelter, J.; Druker, B.; Sawyers, C. L.; Shah, N.; Stock, W.; Willman, C. L.; Friend, S.; Linsley, P. S. Gene expression changes associated with progression and response in chronic myeloid leukemia. *Proc. Natl. Acad. Sci.* **2006**, *103(8)*, 2794–2799.

14. Mischel, P. S.; Cloughesy, T. F.; Nelson, S. F. DNA-microarray analysis of brain cancer: molecular classification for therapy. *Nature Rev. Neuroscience* **2004**, *5*, 782–794.

15. Weinberg, R. A., *Cancer Biology*. Garland Science: 2006.

16. Wysocki, L. J.; Sato, V. L. "Panning" for lymphocytes: a method for cell selection. *Proc. Natl. Acad. Sci.* **1978**, *75(6)*, 2844–2848.

17. Liu, X.; Wang, H.; Herron, J.; Prestwich, G. Photopatterning of antibodies on biosensors. *Bioconjugate Chem.* **2000**, *11*, 755–761.

18. Macbeath, G.; Schreiber, S. L. Printing proteins as microarrays for high-throughput function determination. *Science* **2000**, *289*, 1760–1763.

19. Pal, M.; Moffa, A.; Sreekumar, A.; Ethier, S.; Barder, T.; Chinnaiyan, A.; Lubman, D. Differential phosphoprotein mapping in cancer cells using protein microarrays produced from 2-D liquid fractionation. *Anal. Chem.* **2006**, *78*, 702–710.

20. Thirumalapura, N. R.; Morton, R. J.; Ramachandran, A.; Malayer, J. R. Lipopolysaccharide microarrays for the detection of antibodies. *Journal of Immunological Methods* **2005**, *298*, 73–81.

21. Seigel, R. R.; Harder, P.; Dahint, R.; Grunze, M.; Josse, F.; Mrksich, M.; Whitesides, G. M. On-line detection of nonspecific protein adsorption at artificial surfaces. *Anal. Chem.* **1997**, *69*, 3321–3328.

22. Ramsden, J. J. Puzzles and paradoxes in protein adsorption. *Chem. Soc. Rev.* **1995**, *24*, 73–78.

23. Fainerman, V. B.; Lucassen-Reynders, E.; Miller, R. Adsorption of surfactants and proteins at fluid interfaces. *Colloids Surf. A* **1998**, *143*, 141.

24. Arenkov, P.; Kukhtin, A.; Gemmel, A.; Voloshchuk, S.; Chupeeva, V.; Mirzabekov, A. Protein microchips: use for immunoassay and enzymatic reactions. *Anal. Biochem.* **2000**, *278*, 123–131.

25. Kiyonaka, S.; Sada, K.; Yoshimura, I.; Shinkai, S.; Kato, N.; Hamachi, I. Semi-wet peptide/protein array using supramolecular hydrogel. *Nature Materials* **2004**, *3*, 58–64.

26. Kwon, Y.; Han, Z.; Karatan, E.; Mrksich, M.; Kay, B. K. Antibody arrays prepared by cutinase-mediated immobilization on self-assembled monolayers. *Anal. Chem.* **2004**, *76*, 5713–5720.

27. Peluso, P.; Wilson, D.; Do, D.; Tran, H.; Venkatasubbaiah, M.; Quincy, D.; Heidecker, B.; Poindexter, K.; Tolani, N.; Phelan, M.; Witte, K.; Jung, L.; Wagner, P.; Nock, S. Optimizing antibody immobilization strategies for the construction of protein microarrays. *Anal. Biochem.* **2003**, *312*, 113–124.

28. Chen, D. S.; Soen, Y.; Stuge, T. B.; Lee, P. P.; Weber, J. S.; Brown, P. O.; Davis, M. M. Marked differences in human melanoma antigen-specific T cell responsiveness after vaccination using a functional microarray. *PLoS Medicine* **2005**, *2*, 1018–1030.

29. Soen, Y.; Chen, D. S.; Kraft, D. L.; Davis, M. M.; Brown, P. O. Detection and characterization of cellular immune responses using peptide-MHC microarrays. *PLoS Biology* **2003**, *1(3)*, 429–438.

30. Boozer, C.; Ladd, J.; Chen, S.; Yu, Q.; Homola, J.; Jiang, S. DNA directed protein immobilization on mixed ssDNA/oligo(ethylene glycol) self-assembled monolayers for sensitive biosensors. *Anal. Chem.* **2004**, *76*, 6967–6972.

31. Kozlov, I. A.; Melnyk, P. C.; Stromsborg, K. E.; Chee, M. S.; Barker, D. L.; Zhao, C. Efficient strategies for the conjugation of oligonucleotides to antibodies enabling highly sensitive protein detection. *Biopolymers* **2004**, *73*, 621–630.

32. Adler, M.; Wacker, R.; Booltink, E.; Manz, B.; Niemeyer, C. M. Detection of femtogram amounts of biogenic amines using self-assembled DNA-protein nanostructures. *Nature Methods* **2005**, *2*, 147–149.

33. Sano, T.; Smith, C. L.; Cantor, C. R. Immuno-PCR: very sensitive antigen detection by means of specific antibody-DNA conjugates. *Science* **1992**, *258*, 120–122.

34. Niemeyer, C. M.; Adler, M.; Wacker, R. Immuno-PCR: high sensitivity detection of proteins by nucleic acid amplification. *TRENDS Biotech* **2005**, *23*, 208–216.

35. Wacker, R.; Niemeyer, C. M. DDI-microFIA--A readily configurable microarray-fluorescence immunoassay based on DNA-directed immobilization of proteins. *ChemBioChem* **2004**, *5*, 453–459.

36. Becker, C. F. W.; Wacker, R.; Bouschen, W.; Seidel, R.; Kolaric, B.; Lang, P.; Schroeder, H.; Muller, O.; Niemeyer, C. M.; Spengler, B.; Goody, R. S.; Engelhard, M. Direct readout of protein-protein interactions by mass spectrometry from protein-DNA microarrays. *Angew. Chem.* **2005**, *44*, 7635–7639.

37. Boozer, C.; Ladd, J.; Chen, S.; Jiang, S. DNA-Directed Protein Immobilization for Simultaneous Detection of Multiple Analytes by Surface Plasmon Resonance Biosensor. *Anal. Chem.* **2006**, *78*, 1515–1519.

38. Dirks, R. M.; Lin, M.; Winfree, E.; Pierce, N. A. Paradigms for computational nucleic acid design. *Nucleic Acids Research* **2004**, *32(4)*, 1392–1403.

39. Groves, T.; Katis, P.; Madden, Z.; Manickam, K.; Ramsden, D.; Wu, G.; Guidos, C. J. In vitro maturation of clonal CD4+CD8+ cell lines in response to TCR engagement. *J. Immunol.* **1995**, *154*, 5011–5022.

40. Kim, K. J.; Langevin, C. K.; Merwin, R. M.; Sachs, D. H.; Asfsky, R. Establishment and characterization of BALB/c lymphoma lines with B cell properties. *J. Immunol.* **1979**, *122*, 549–554.

41. This approach to conjugate synthesis is expected to result in a distribution of DNA loadings for each antibody, however, we feel as this effect is exaggerated in preparation for PAGE analysis. We observed that normal conditions for the heat-induced denaturation proceeding gel electrophoresis (100^{o} for 5 minutes) reduced the number of DNA-strands visualized, presumably by breaking the hydrazone

linkage between the DNA and the protein. By relaxing the denaturing conditions, a sample heated at 60^{o} for 5 minutes (minimum required for good gel) showed up to 7 discrete bands, whereas the same sample heated at 100^{o} for 5 minutes showed no pendant oligonucleotides.

42. Prime, K. L.; Whitesides, G. M. Self-assembled organic monolayers: model systems for studying adsorption of proteins at surfaces. *Science* **1991**, *252*, 1164–1167.

43. Prime, K. L.; Whitesides, G. M. Adsorption of proteins onto surfaces containing end-attached oligo(ethylene oxide): a model system using self-assembled monolayers. *J. Am. Chem. Soc.* **1993**, *115(23)*, 10714 – 10721.

44. Jeon, S. I.; Lee, J. H.; Andrade, J. D.; De Gennes, P. G. Protein-surface interactions in the presence of polyethylene oxide. I. Simplified theory. *Journal of Colloid and Interface Science* **1991**, *142(1)*, 149–158.

45. Jeon, S. I.; Andrade, J. D. Protein-surface interactions in the presence of polyethylene oxide. II. Effect of protein size. *Journal of Colloid and Interface Science* **1991**, *142(1)*, 159–166.

46. Andrade, J. D.; Hlady, V. Protein adsorption and materials biocompatibility: a tutorial review and suggested hypotheses. *Advances in Polymer Science* **1986**, *79*, (1–63).

47. Breslauer, D. N.; Lee, P. J.; Lee, L. P. Microfluidics-based systems biology. *Mol. BioSyst.* **2006**, *2*, 97–112.

48. Zimmermann, M.; Delamarche, E.; Wolf, M.; Hunziker, P. Modeling and optimization of high-sensitivity, low-volume microfluidic-based surface immunoassays. *Biomedical Microdevices* **2005**, *7(2)*, 99–110.

49. Erickson, D.; Li, D.; Krull, U. Modeling of DNA hybridization kinetics for spatially resolved biochips. *Anal. Biochem.* **2003**, *317*, 186–200.

50. Bunimovich, Y.; Shin, Y.; Yeo, W.; Amori, M.; Kwong, G.; Heath, J. Quantitative real-time measurements of DNA hybridization with alkylated nonoxidized silicon nanowires in electrolyte solution. *J. Am. Chem. Soc.* **2006**, *128(50)*, 16323–16331.

51. Wei, C.; Cheng, J.; Huang, C.; Yen, M.; Young, T. Contextual interactions determine whether the Drosophila homeodomain protein, Vnd, acts as a repressor or activator. *Nucleic Acids Research* **2005**, *33(8)*, 1–11.

52. Engvall, E.; Perlmann, P. O. Enzyme-linked immunosorbent assay, Elisa. 3. Quantitation of specific antibodies by enzyme-labeled anti-immunoglobulin in antigen-coated tubes. *J. Immunol.* **1972**, *109*, 129–135.

53. Pirrung, M. How to make a DNA chip. *Angew. Chem. Int. Ed.* **2002**, *41*, 1276–1289.

54. Hainfeld, J. F.; Powell, R. D., Silver- and Gold-Based Autometallography of Nanogold. In *Gold and Silver Staining: Techniques in Molecular Morphology*, Hacker, G. W.; Gu, J., Eds. CRC Press: Washington, DC, 2002; pp 29–46.

55. Crowther, J. R., ELISA; Theory and Practice. In *Methods in Molecular Biology*, Humana Press Inc.: Totowa, New Jersey, 1995.

56. http://www.bdbiosciences.com/ptProduct.jsp?prodId=6725.

57. Thibault, C.; Le Berre, V.; Casimirius, S.; Tervisiol, E.; Francois, J.; Vieu, C. Examination of Cholesterol oxidase attachment to magnetic nanoparticles. *Journal of Nanobiotechnology* **2005**, *3(7)*, 1–12.

58. Cardoso, A. A.; Watt, S. M.; Batard, P.; Li, M. L.; Hatzfeld, A.; Genevier, H.; Hatzfeld, J. An improved panning technique for the selection of CD34+ human bone marrow hematopoietic cells with high recovery of early progenitors. *Exp. Hematol.* **1995**, *23*, 407–412.

59. Taton, T. A.; Mirkin, C. A.; Letsinger, R. L. Scanometric DNA array detection with nanoparticle probes. *Science* **2000**, *289*, 1757–1760.

60. Campbell, R. E.; Tour, O.; Palmer, A. E.; Steinbach, P. A.; Baird, G. S.; Zacharias, D. A.; Tsien, R. Y. A monomeric red fluorescent protein. *Proc. Natl. Acad. Sci.* **2002**, *99*, 7877–7882.

61. Soen, Y.; Chen, D. S.; Kraft, D. L.; Davis, M. M.; Brown, P. O. Detection and characterization of cellular immune responses using peptide-MHC microarrays. *PLos Biology* **2003**, *1*, 429–438.

2.6 Appendix A: Computational derivation of Orthogonal DNA oligomers

There are several applications of the computational algorithm developed by Dirks et al. (38). First it can accept a list of sequences (`A, B, C, … n`) and return with an exhaustive file listing the relative interaction strengths between any two DNA sequences. This value, reported as `n(s*)`, roughly represents the orthogonality of the two sequences that are being compared. As an example, sequences A1, B1 and C1 (inputs as `A`, `B`, and `C` respectively) were analyzed and the results are listed in **Appendix 2.6.1**. Here, the interaction strength of sequence `B` with `B`, representing intra-strand interactions, has the lowest `n(s*)` value of `7.525723`, and thus is the most orthogonal pair. In comparison, the interaction strength of `An` with `An` (`n` represents the complement operator) has the highest `n(s*)` value of `16.406083` and thus is the least orthogonal pair. A good measure of the global orthogonality of a set of sequences is determined by the set with the lowest Σ `n(s*)`.

Besides analysis, a set of sequences can be generated by inputing a set of constraints (e.g. sequence length, defined sequences, etc.) and the program will return with a set of sequences ranked according to `n(s*)` adhering to the given constraints. An example of this is given by the input file shown in **Appendix 2.6.2**, where the input code asks for 3 orthogonal sequences (`A, B, and C`) such that each sequences begins with a polyA_{10} header before a variable 20mer region. The set of sequences (truncated to show only 3 sets of 10 total) with the lowest `n(s*)` value of `149.225` was taken and defined to be A3, B3 and C3, the sequences used in this chapter (**Appendix 2.6.3**). This

process can be repeated iteratively to increase the number of orthogonal sequences. Example input (**Appendix 2.6.4**) and output (**Appendix 2.6.5**) is given for the computation of a fourth DNA sequence.

2.6.1 Computational analysis of sequence A1, B1, and C1

```
Results sorted by n(s*) sum

A_A:
AAAAAAAAAACGTGACATCATGCATG+AAAAAAAAAACGTGACATCATGCATG 15.893007
.........................+......................... <- target
..................(((((((+.................)))))))) <- predicted
An_An:
AAAAAAAAAACATGCATGATGTCACG+AAAAAAAAAACATGCATGATGTCACG 16.406083
.........................+......................... <- target
..........(((((((((........+..........)))))))).......... <- predicted
An_Bn:
AAAAAAAAAACATGCATGATGTCACG+AAAAAAAAAAACTGGTATGCGAATCC 9.679928
.........................+......................... <- target
.........................+......................... <- predicted
An_Cn:
AAAAAAAAAACATGCATGATGTCACG+AAAAAAAAAAATGTGCAATGCGTCCA 11.736368
.........................+......................... <- target
.........................+......................... <- predicted
An_B:
AAAAAAAAAACATGCATGATGTCACG+AAAAAAAAAAGGATTCGCATACCAGT 10.011576
.........................+......................... <- target
...........((((...........+..............)))).....  <- predicted
An_C:
AAAAAAAAAACATGCATGATGTCACG+AAAAAAAAAATGGACGCATTGCACAT 13.267340
.........................+......................... <- target
.........................+......................... <- predicted
B_B:
AAAAAAAAAAGGATTCGCATACCAGT+AAAAAAAAAAGGATTCGCATACCAGT 7.525723
.........................+......................... <- target
.........................+......................... <- predicted
Bn_Bn:
AAAAAAAAAAACTGGTATGCGAATCC+AAAAAAAAAAACTGGTATGCGAATCC 8.707963
.........................+......................... <- target
..................((.....+..................)).....  <- predicted
Bn_Cn:
AAAAAAAAAAACTGGTATGCGAATCC+AAAAAAAAAAATGTGCAATGCGTCCA 9.372607
.........................+......................... <- target
.........................+......................... <- predicted
Bn_A:
AAAAAAAAAAACTGGTATGCGAATCC+AAAAAAAAAACGTGACATCATGCATG 9.717578
.........................+......................... <- target
...............((((......+...................)))). <- predicted
Bn_C:
```

```
AAAAAAAAAAACTGGTATGCGAATCC+AAAAAAAAAATGGACGCATTGCACAT 12.147723
.........................+..........................  <- target
...............(((((.....+.............)))))........  <- predicted
C_C:
AAAAAAAAAATGGACGCATTGCACAT+AAAAAAAAAATGGACGCATTGCACAT 14.639235
.........................+..........................  <- target
..............(((.(((....+.............))).)))....  <- predicted
Cn_Cn:
AAAAAAAAAAATGTGCAATGCGTCCA+AAAAAAAAAAATGTGCAATGCGTCCA 14.117287
.........................+..........................  <- target
..............(((.(((.....+.............))).))).....  <- predicted
Cn_A:
AAAAAAAAAAATGTGCAATGCGTCCA+AAAAAAAAAACGTGACATCATGCATG 12.522849
.........................+..........................  <- target
.........................+..........................  <- predicted
Cn_B:
AAAAAAAAAAATGTGCAATGCGTCCA+AAAAAAAAAAGGATTCGCATACCAGT 15.107010
.........................+..........................  <- target
................(((((((((.+.........)))..)))))).....  <- predicted
D:
C 0.000000
. <- target
. <- predicted
Total n(s*) = 180.852
```

2.6.2 Computing orthogonal sequences A, B, and C constrained by a polyA$_{10}$ header: input file

```
R: 10, 20, 20, 20        %%Defining R to contain 10, or 20 bases
R1: AAAAAAAAAA           %%Defining the first 10 bases to be polyA10

A_A: 1, 2, 1, 2          %%Sequence A is composed of R1 = polyA10, and R2
                         which is variable 20 mer
............................+............................
An_An: 1, -2, 1, -2
............................+............................
An_Bn: 1, -2, 1, -3
............................+............................
An_Cn: 1, -2, 1, -4
............................+............................
An_B: 1, 2, 1, 3
............................+............................
An_C: 1, 2, 1, 4
............................+............................
B_B: 1, 3, 1, 3
............................+............................
Bn_Bn: 1, -3, 1, -3
............................+............................
Bn_Cn: 1, -3, 1, -4
............................+............................
Bn_A: 1, -3, 1, 2
```

```
.............................+.............................
Bn_C: 1, -3, 1, 4
.............................+.............................
C_C: 1, 4, 1, 4
.............................+.............................
Cn_Cn: 1, -4, 1, -4
.............................+.............................
Cn_A: 1, -4, 1, 2
.............................+.............................
Cn_B: 1, -4, 1, 3
.............................+.............................
```

2.6.3 PolyA$_{10}$ header computational results

```
Results sorted by n(s*) sum

A_A:
AAAAAAAAAACGTGCCTACGGATCATTCTA+AAAAAAAAAACGTGCCTACGGATCATTCTA 14.752380
.............................+.............................. <- target
..........(((....)))..........+..........(((....)))........... <- predicted
An_An:
AAAAAAAAAATAGAATGATCCGTAGGCACG+AAAAAAAAAATAGAATGATCCGTAGGCACG 12.191140
.............................+.............................. <- target
.............................+.............................. <- predicted
An_Bn:
AAAAAAAAAATAGAATGATCCGTAGGCACG+AAAAAAAAAATACGAGCTACTAAGTGTCCG 10.821610
.............................+.............................. <- target
.............................+.............................. <- predicted
An_Cn:
AAAAAAAAAATAGAATGATCCGTAGGCACG+AAAAAAAAAATACCGAGTCAGGACCGTCGC 11.704642
.............................+.............................. <- target
..................((...)).....+.............................. <- predicted
An_B:
AAAAAAAAAATAGAATGATCCGTAGGCACG+AAAAAAAAAACGGACACTTAGTAGCTCGTA 12.387949
.............................+.............................. <- target
..................(((((.......+.........)))))................ <- predicted
An_C:
AAAAAAAAAATAGAATGATCCGTAGGCACG+AAAAAAAAAAGCGACGGTCCTGACTCGGTA 13.792005
.............................+.............................. <- target
..................((((..((...+..........)).))))............. <- predicted
B_B:
AAAAAAAAAACGGACACTTAGTAGCTCGTA+AAAAAAAAAACGGACACTTAGTAGCTCGTA 15.189105
.............................+.............................. <- target
.............................+.............................. <- predicted
Bn_Bn:
AAAAAAAAAATACGAGCTACTAAGTGTCCG+AAAAAAAAAATACGAGCTACTAAGTGTCCG 10.362398
.............................+.............................. <- target
.............................+.............................. <- predicted
Bn_Cn:
AAAAAAAAAATACGAGCTACTAAGTGTCCG+AAAAAAAAAATACCGAGTCAGGACCGTCGC 11.009212
.............................+.............................. <- target
...........((.................+.......................)).... <- predicted
Bn_A:
AAAAAAAAAATACGAGCTACTAAGTGTCCG+AAAAAAAAAACGTGCCTACGGATCATTCTA 11.155809
.............................+.............................. <- target
.............................+.............................. <- predicted
```

```
Bn_C:
AAAAAAAAAATACGAGCTACTAAGTGTCCG+AAAAAAAAAAGCGACGGTCCTGACTCGGTA 12.599213
.............................+............................. <- target
............((((.............+.......................)))).... <- predicted
C_C:
AAAAAAAAAAGCGACGGTCCTGACTCGGTA+AAAAAAAAAAGCGACGGTCCTGACTCGGTA 22.259374
.............................+............................. <- target
.........(.(((..(((..((((((.(.+.........).)))..)))..)))))).). <- predicted
Cn_Cn:
AAAAAAAAAATACCGAGTCAGGACCGTCGC+AAAAAAAAAATACCGAGTCAGGACCGTCGC 15.521820
.............................+............................. <- target
..................(..(........+..................)..)........ <- predicted
Cn_A:
AAAAAAAAAATACCGAGTCAGGACCGTCGC+AAAAAAAAAACGTGCCTACGGATCATTCTA 12.952999
.............................+............................. <- target
.......................((((...+................)))).......... <- predicted
Cn_B:
AAAAAAAAAATACCGAGTCAGGACCGTCGC+AAAAAAAAAACGGACACTTAGTAGCTCGTA 13.708535
.............................+............................. <- target
.......................((((...+.........)))).................. <- predicted
Total n(s*) = 200.408

...

A_A:
AAAAAAAAAAATCAAGTAGCGAATGGACTA+AAAAAAAAAAATCAAGTAGCGAATGGACTA 7.851744
.............................+............................. <- target
.............................+............................. <- predicted
An_An:
AAAAAAAAAATAGTCCATTCGCTACTTGAT+AAAAAAAAAATAGTCCATTCGCTACTTGAT 10.114856
.............................+............................. <- target
.............................+............................. <- predicted
An_Bn:
AAAAAAAAAATAGTCCATTCGCTACTTGAT+AAAAAAAAAATACCGTGAAGCGTCCTAGTA 11.335990
.............................+............................. <- target
...................((((.......+.................)))).......... <- predicted
An_Cn:
AAAAAAAAAATAGTCCATTCGCTACTTGAT+AAAAAAAAAATAGATACGATGGCTCAGTGC 11.862416
.............................+............................. <- target
..............(..............+...................)......... <- predicted
An_B:
AAAAAAAAAATAGTCCATTCGCTACTTGAT+AAAAAAAAAATACTAGGACGCTTCACGGTA 11.058647
.............................+............................. <- target
.............................+............................. <- predicted
An_C:
AAAAAAAAAATAGTCCATTCGCTACTTGAT+AAAAAAAAAAGCACTGAGCCATCGTATCTA 10.700609
.............................+............................. <- target
.............................+............................. <- predicted
B_B:
AAAAAAAAAATACTAGGACGCTTCACGGTA+AAAAAAAAAATACTAGGACGCTTCACGGTA 14.394146
.............................+............................. <- target
............((((..((.....))...+............))))..((.....))... <- predicted
Bn_Bn:
AAAAAAAAAATACCGTGAAGCGTCCTAGTA+AAAAAAAAAATACCGTGAAGCGTCCTAGTA 13.083925
.............................+............................. <- target
.............................+............................. <- predicted
Bn_Cn:
AAAAAAAAAATACCGTGAAGCGTCCTAGTA+AAAAAAAAAATAGATACGATGGCTCAGTGC 12.305284
.............................+............................. <- target
...................(((.......+..............)))....(.....). <- predicted
```

```
Bn_A:
AAAAAAAAAATACCGTGAAGCGTCCTAGTA+AAAAAAAAAAATCAAGTAGCGAATGGACTA 9.982085
.............................+.............................. <- target
.....................(........+...........................).. <- predicted
Bn_C:
AAAAAAAAAATACCGTGAAGCGTCCTAGTA+AAAAAAAAAAGCACTGAGCCATCGTATCTA 10.427249
.............................+.............................. <- target
.............................+.............................. <- predicted
C_C:
AAAAAAAAAAGCACTGAGCCATCGTATCTA+AAAAAAAAAAGCACTGAGCCATCGTATCTA 8.990198
.............................+.............................. <- target
.............................+.............................. <- predicted
Cn_Cn:
AAAAAAAAAATAGATACGATGGCTCAGTGC+AAAAAAAAAATAGATACGATGGCTCAGTGC 9.885630
.............................+.............................. <- target
...............((....(.....).+...............))....(.....). <- predicted
Cn_A:
AAAAAAAAAATAGATACGATGGCTCAGTGC+AAAAAAAAAAATCAAGTAGCGAATGGACTA 9.740523
.............................+.............................. <- target
.............................+.............................. <- predicted
Cn_B:
AAAAAAAAAATAGATACGATGGCTCAGTGC+AAAAAAAAAAATACTAGGACGCTTCACGGTA 10.394821
.............................+.............................. <- target
.............................+..................((.....))... <- predicted
Total n(s*) = 162.128

...

A_A:
AAAAAAAAAAATCCTGGAGCTAAGTCCGTA+AAAAAAAAAAATCCTGGAGCTAAGTCCGTA 11.081137
.............................+.............................. <- target
............((.((............+............)).))............. <- predicted
An_An:
AAAAAAAAAATACGGACTTAGCTCCAGGAT+AAAAAAAAAATACGGACTTAGCTCCAGGAT 11.417329
.............................+.............................. <- target
.....................((........+...................)).......... <- predicted
An_Bn:
AAAAAAAAAATACGGACTTAGCTCCAGGAT+AAAAAAAAAAATAGGCATGATTCAATGAGGC 9.031869
.............................+.............................. <- target
.............................+.............................. <- predicted
An_Cn:
AAAAAAAAAATACGGACTTAGCTCCAGGAT+AAAAAAAAAAATAGCGATAGTAGACGAGTGC 9.887457
.............................+.............................. <- target
.............................+.............................. <- predicted
An_B:
AAAAAAAAAATACGGACTTAGCTCCAGGAT+AAAAAAAAAAGCCTCATTGAATCATGCCTA 9.893760
.............................+.............................. <- target
.............................+.............................. <- predicted
An_C:
AAAAAAAAAATACGGACTTAGCTCCAGGAT+AAAAAAAAAAGCACTCGTCTACTATCGCTA 9.416199
.............................+.............................. <- target
.............................+.............................. <- predicted
B_B:
AAAAAAAAAAGCCTCATTGAATCATGCCTA+AAAAAAAAAAGCCTCATTGAATCATGCCTA 10.372686
.............................+.............................. <- target
.............................+.............................. <- predicted
Bn_Bn:
AAAAAAAAAATAGGCATGATTCAATGAGGC+AAAAAAAAAATAGGCATGATTCAATGAGGC 11.143822
.............................+.............................. <- target
..............((.............+..............))............. <- predicted
```

```
Bn_Cn:
AAAAAAAAAATAGGCATGATTCAATGAGGC+AAAAAAAAAATAGCGATAGTAGACGAGTGC 9.725931
.............................+............................. <- target
.............................+............................. <- predicted
Bn_A:
AAAAAAAAAATAGGCATGATTCAATGAGGC+AAAAAAAAAAATCCTGGAGCTAAGTCCGTA 9.849003
.............................+............................. <- target
.............................+............................. <- predicted
Bn_C:
AAAAAAAAAATAGGCATGATTCAATGAGGC+AAAAAAAAAAGCACTCGTCTACTATCGCTA 10.070369
.............................+............................. <- target
.............................+............................. <- predicted
C_C:
AAAAAAAAAAGCACTCGTCTACTATCGCTA+AAAAAAAAAAGCACTCGTCTACTATCGCTA 8.656702
.............................+............................. <- target
.............................+............................. <- predicted
Cn_Cn:
AAAAAAAAAATAGCGATAGTAGACGAGTGC+AAAAAAAAAATAGCGATAGTAGACGAGTGC 9.905828
.............................+............................. <- target
.............................+............................. <- predicted
Cn_A:
AAAAAAAAAATAGCGATAGTAGACGAGTGC+AAAAAAAAAAATCCTGGAGCTAAGTCCGTA 9.691171
.............................+............................. <- target
......................(((.....+.........................))). <- predicted
Cn_B:
AAAAAAAAAATAGCGATAGTAGACGAGTGC+AAAAAAAAAAGCCTCATTGAATCATGCCTA 9.081401
.............................+............................. <- target
.............................+............................. <- predicted
Total n(s*) = 149.225
```

2.6.4 Computing a fourth sequence: input code

```
>Test #6
R: 10, 20, 20, 20, 20
R1: AAAAAAAAAA
R2: ATCCTGGAGCTAAGTCCGTA
R3: GCCTCATTGAATCATGCCTA
R4: GCACTCGTCTACTATCGCTA

D_D: 1, 5, 1, 5
.............................+.............................
Dn_A: 1, -5, 1, 2
.............................+.............................
Dn_B: 1, -5, 1, 3
.............................+.............................
Dn_C: 1, -5, 1, 4
.............................+.............................
Dn_An: 1, -5, 1, -2
.............................+.............................
Dn_Bn: 1, -5, 1, -3
.............................+.............................
Dn_Cn: 1, -5, 1, -4
.............................+.............................
Dn_Dn: 1, -5, 1, -5
.............................+.............................
```

2.6.5 Results of fourth strand computation

```
D_D:
AAAAAAAAAAATGGTCGAGATGTCAGAGTA+AAAAAAAAAAATGGTCGAGATGTCAGAGTA 10.604201
.............................+............................. <- target
..............((............+............))............. <- predicted
Dn_A:
AAAAAAAAAATACTCTGACATCTCGACCAT+AAAAAAAAAAATCCTGGAGCTAAGTCCGTA 7.984174
.............................+............................. <- target
.............................+............................. <- predicted
Dn_B:
AAAAAAAAAATACTCTGACATCTCGACCAT+AAAAAAAAAAGCCTCATTGAATCATGCCTA 6.890737
.............................+............................. <- target
.............................+............................. <- predicted
Dn_C:
AAAAAAAAAATACTCTGACATCTCGACCAT+AAAAAAAAAAGCACTCGTCTACTATCGCTA 6.684232
.............................+............................. <- target
.............................+............................. <- predicted
Dn_An:
AAAAAAAAAATACTCTGACATCTCGACCAT+AAAAAAAAAATACGGACTTAGCTCCAGGAT 7.998166
.............................+............................. <- target
.............................+............................. <- predicted
Dn_Bn:
AAAAAAAAAATACTCTGACATCTCGACCAT+AAAAAAAAAATAGGCATGATTCAATGAGGC 9.261694
.............................+............................. <- target
.............................+............................. <- predicted
Dn_Cn:
AAAAAAAAAATACTCTGACATCTCGACCAT+AAAAAAAAAATAGCGATAGTAGACGAGTGC 11.865802
.............................+............................. <- target
.....................((((.....+.....................))))... <- predicted
Dn_Dn:
AAAAAAAAAATACTCTGACATCTCGACCAT+AAAAAAAAAATACTCTGACATCTCGACCAT 6.770436
.............................+............................. <- target
......................((.....+.....................)).....  <- predicted
Total n(s*) = 68.059
```

2.7 Appendix B: FPLC of DEAL conjugates.

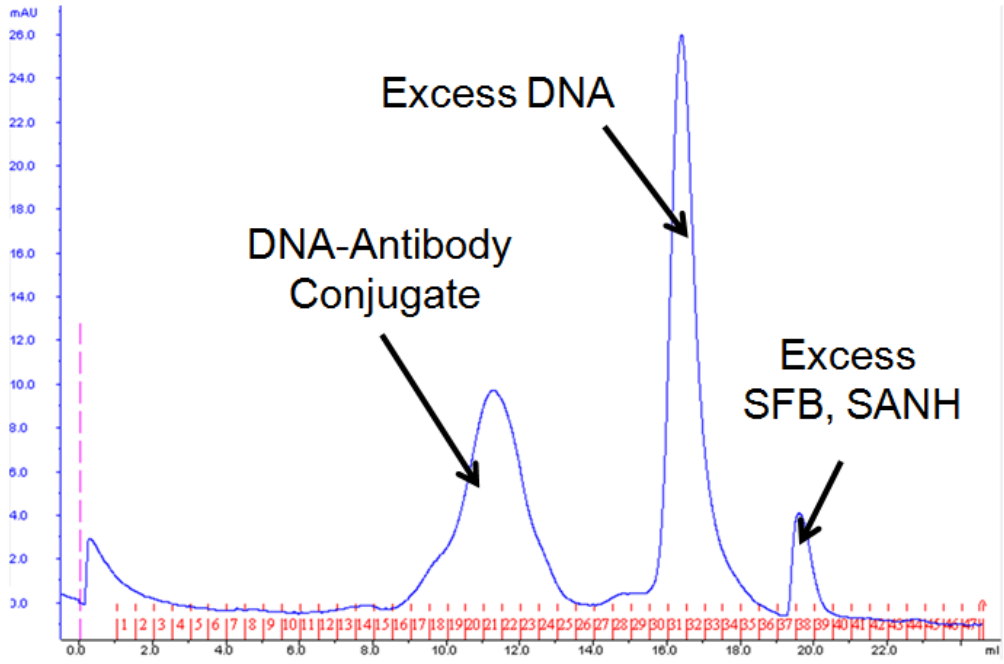

*0.5 mL/min isocratic flow of PBS

Figure 2.11 Fast protein liquid chromatography of DEAL conjugates. A typical successful conjugation reaction will yield three distinct peaks, corresponding to the DEAL conjugates, excess unreacted ssDNA, and excess small molecules.